coatings

MDPI

Article

Adhesion Improvement Between Cu-Etched Commercial Polyimide/Cu Foils and Biopolymers for Sustainable In-Mold Electronics

Zahra Fazlali [1,*], David Schaubroeck [1,*], Maarten Cauwe [1], Karen Leus [2], Rino Morent [2], Nathalie De Geyter [2], Ludwig Cardon [3], Pieter Bauwens [1] and Jan Vanfleteren [1]

[1] Centre for Microsystems Technology, Imec, Ghent University, Technology Park 126, B-9052 Gent-Zwijnaarde, Belgium; maarten.cauwe@ugent.be (M.C.); pieter.bauwens@ugent.be (P.B.); jan.vanfleteren@ugent.be (J.V.)
[2] Research Unit Plasma Technology (RUPT), Department of Applied Physics, Ghent University, Sint-Pietersnieuwstraat 41 B4, B-9000 Gent, Belgium; karen.leus@ugent.be (K.L.); rino.morent@ugent.be (R.M.); nathalie.degeyter@ugent.be (N.D.G.)
[3] Centre for Polymer and Material Technologies (CPMT), Ghent University, Technology Park 130, B-9052 Gent-Zwijnaarde, Belgium; ludwig.cardon@ugent.be
* Correspondence: zahra.fazlali@ugent.be (Z.F.); david.schaubroeck@ugent.be (D.S.)

Abstract

Embedding flexible electronic circuits into a sustainable polymer is an emerging and significant topic in the field of in-mold electronics (IME). Ensuring strong adhesion between the flexible circuit and the molded polymer is critical for the durability of IME products. In this study, three different types of etched copper polyimide (PI) foils were used as the substrate of electronic components. Two bio-based and biodegradable polymers of polylactic acid (PLA) and polyhydroxybutyrate (PHB) served as the overmolding material. Four different surface pretreatments: drying, polydopamine (PDA) coating, PDA coating followed by thermal treatment under vacuum, oxygen plasma, and 3-aminopropyltriethoxysilane (APTES) were applied to the PI surface prior to the overmolding process to investigate the influence on the adhesive strength. Additionally, a thermoplastic polyurethane (TPU) adhesive layer was introduced via vacuum lamination to further improve adhesion. The main objective of this study was to evaluate the adhesive strength between etched PI and overmolded biopolymers before and after surface modifications. The loci of failure were analyzed using scanning electron microscopy (SEM). The results indicate that laminated TPU is the most effective approach for improving adhesion between polyimide foils and biopolymers.

Keywords: in-mold electronics (IME); adhesion; surface treatment; sustainable electronics; polyimide; polylactic acid (PLA); polyhydroxybutyrate (PHB)

Academic Editor: Anna Palau

Received: 30 June 2025
Revised: 9 December 2025
Accepted: 15 December 2025
Published: 17 December 2025

Citation: Fazlali, Z.; Schaubroeck, D.; Cauwe, M.; Leus, K.; Morent, R.; De Geyter, N.; Cardon, L.; Bauwens, P.; Vanfleteren, J. Adhesion Improvement Between Cu-Etched Commercial Polyimide/Cu Foils and Biopolymers for Sustainable In-Mold Electronics. *Coatings* **2025**, *15*, 1489. https://doi.org/10.3390/coatings15121489

1. Introduction

The growing demand for lighter, more compact, and shapeable electronic devices with simplified manufacturing has driven the development of technologies integrating plastics and electronics. In-mold electronics (IME) is an emerging technology that enables the integration of electronic functionality into polymer materials. The IME process consists of four steps: patterning conductive traces on a flexible polymer carrier, component assembly, thermoforming, and overmolding [1,2]. Manufacturing electronic parts with IME technology requires less material and assembly effort compared to conventional methods such as Laser Direct Structuring (LDS). Furthermore, this technology provides greater design flexibility to create more sophisticated functional devices. Therefore, it is an easy

and cost-effective approach. These advantages make IME highly attractive for a wide range of applications, including automotive interiors, wearable electronics, household devices, and medical applications [3].

Despite these advantages, IME presents sustainability and environmental challenges like other electronic products. Typically, these hybrid electronics end up in the recycling shredders or incinerators to recover the (precious) metals. However, recycling these hybrid structures is highly energy-intensive due to the complex combination of polymers, fillers, and metals, and the process often generates large amounts of greenhouse gases (GHG). Moreover, a significant portion of them ends up in landfills, contributing to electronic waste (e-waste) accumulation and creating environmental and health hazards [4,5].

One promising approach to reduce the environmental footprint of IME technology is the replacement of petroleum-based polymers with biopolymers [6]. Since polymers represent the largest fraction of e-waste, adopting biodegradable and bio-based materials can significantly reduce long-term pollution and waste disposal issues [7]. Biopolymers generally require fewer toxic additives during processing, making them safer for both the environment and human health [8].

Biopolymers refer to polymers that are either bio-based and/or biodegradable. Bio-based polymers are derived from renewable and biological sources, while conventional polymer precursors are made from crude oil-derived molecules. On the other hand, biodegradability refers to the polymer's end of life, meaning that it can naturally decompose into non-toxic byproducts (e.g., water, CO_2, and biomass) through microbial activity [9]. Biodegradable polymers can be bio-based or petroleum-derived.

Over the past decades, various bio-based/biodegradable polymers have been developed and produced for different applications. Polylactic acid (PLA) is a popular thermoplastic polyester derived from renewable sources such as corn, sugarcane, etc. The starch or sugar is fermented to produce lactic acid monomers. PLA is synthesized via polycondensation of lactic acid [10]. Its attractive properties, such as biocompatibility, biodegradability, low shrinkage, and low processing temperature, made PLA a leading candidate for many applications, such as food packaging [11] and biomedical materials [12]. Another well-known bio-based and biodegradable polymer is polyhydroxybutyrate (PHB) [13]. In terms of mechanical properties, PHB is generally stiffer and more brittle than PLA. The properties of PHB are similar to those of several petroleum-derived polymers, such as polypropylene (PP) and polyethylene (PE) (Table 1) [14,15]. Using PLA and PHB as overmolding materials in IME offers potential benefits by reducing plastic waste, as they can be biodegraded in nature or composted. Moreover, the overall CO_2 emission is reduced due to CO_2 absorption during the plant (e.g., corn) growth [16].

Table 1. Properties of polymers (as an overmolding material).

Properties	PP	PE	PLA	PHB
Density (g/cm^3)	0.91–0.94	0.9–0.97	1.25	1.23
Tensile Strength (MPa)	20–40	10–30	21–60	20–40
Elongation at Break (%)	3–700	90–700	3–30	5–8
Young's Modulus (GPa)	1.5–2	0.2–1.0	3.0–4.0	3–3.5
Melting Point (°C)	160–170	105–135	150–180	165–175

The electronic functionality of IME devices is made using flexible polymer carriers. Various polymer foils, including polyimide (PI), polyethylene terephthalate (PET), and polyethylene naphthalate (PEN), have been used as substrates for flexible circuits. Among them, PI stands out due to its excellent thermal stability, mechanical strength, chemical resistance, and flexibility [17]. Furthermore, PI is compatible with standard printed circuit

board (PCB) manufacturing and assembly technologies, allowing it to withstand harsh chemical processes and high soldering temperatures (200–250 °C) [18].

To ensure the functionality and durability of IMEs, a strong interfacial bond between the (etched) copper PI foil and overmolded biopolymers is crucial [19,20]. Adhesion at the polymer–polymer interface is influenced by molecular interactions and surface roughness [21,22]. Various physical and chemical treatments have been employed to improve PI adhesion. Cen-Puc et al. investigated the effects of reactive ion etching and chemical etching on PI adhesion performance [23].

Mashayekhi et al. demonstrated that a combination of plasma activation and adhesive nanocoating using polydopamine can significantly improve adhesion between PI and PLA in a sensor packaging context [24]. A recent study by Kafkopoulos et al. investigated the role of annealing temperature on polydopamine-coated metal–PLA interfaces and showed that a thermal posttreatment in vacuum at 50 °C results in increased interfacial energy of adhesion. Higher temperatures lead to a decrease. This thermal treatment step allows tuning the surface reactive chemical groups of the PDA and provides a certain control over the adhesion [25]. These findings support the importance of PDA surface chemistry in improving adhesion.

This study compares different surface treatment strategies to enhance adhesion between three commercially available PI foils (containing an adhesive layer) obtained after complete Cu etching and overmolded biopolymers (PLA and PHB). The treatments studied include the following:

1. drying the PI in an oven;
2. polydopamine (PDA) coating;
3. polydopamine coating followed by thermal treatment at 50 °C in vacuum;
4. oxygen plasma surface activation;
5. treatment of the PI with a silane adhesion promoter;
6. lamination of a TPU adhesive tie layer.

The general reasoning behind the surface modification treatments (two to five) is to introduce amine and hydroxyl groups on the surface. These are able to react with the ester groups present in each polymer unit of PLA and PHB during the overmolding, resulting in a covalent bond between the modified foils and the overmolded polymer. Of course, other chemical or physical interactions between the two materials can also be established.

Several surface analysis methods, including water contact angle (WCA), scanning electron microscopy (SEM), and optical profilometry, were utilized to assess the effects of the treatments on the wettability and roughness. Moreover, X-ray photoelectron spectroscopy (XPS) was used to analyze surface chemical compositions of the PI foils before and after the surface treatments. Finally, 180-degree peel tests were conducted to quantify and compare adhesion performance.

2. Materials

In this study, three commercial Cu cladding PI foils have been used as starting substrates. One of these foils is just a layer of PI and copper. Two of them, however, contain three layers: PI, adhesive, and copper. The adhesive layer is intended to bond the PI and Cu layers. The layer compositions and thicknesses of the three foils are illustrated in Table 2. The Upisel-N SR1220 (hereinafter referred to as Upisel) foil was purchased from UBE Europe GmbH, Düsseldorf, Germany, the Pyralux FR9120R (hereinafter referred to as Pyralux) was supplied by DuPont, DE, USA, and the Shengyi SF305R (hereinafter referred to as Shengyi) was obtained from SYTECH (China).

Table 2. Build-up of the three Cu cladding PI foils used in this work [26].

Flexible Foil Layers	Upisel-N SR1220	Pyralux FR9120R	Shengyi SF305R
Polyimide (PI)	50 µm	50 µm	25 µm
Adhesive	No adhesive layer	25 µm acrylic-based adhesive	20 µm epoxy-based adhesive
Copper (Rolled-annealed)	18 µm	35 µm	18 µm

Typically, the largest area of the flexible circuit surface after copper patterning consists of PI or adhesive on PI. Therefore, this study aims to evaluate the adhesion of PI foils after complete etching of the Cu layer. To achieve this, the three foils were spray-etched to remove all copper. The spray etcher used in this work is a Sprint 3000US, Windeck, Germany. The etchant is a solution of $CuCl_2 \cdot 2H_2O$ and HCl heated to 35 °C.

Concerning the overmolding material, PLA 3100HP was supplied by NatureWorks, MN, USA, in pellet form. PHB P263E was purchased from Biomer, Schwalbach, Germany, in pellet form.

The polydopamine coating solution consisted of phosphate-buffered saline (PBS) P4417-50TAB (Sigma-Aldrich, MO, USA) and dopamine hydrochloride H8502-10G powder (Sigma-Aldrich, Hessen, Germany). The adhesion promoter 3-aminopropyltriethoxysilane (APTES) was purchased from Sigma-Aldrich (USA). The Bemis 3914 TPU tie layer with a 100 µm thickness was obtained from Bemis Associates Inc. (MA, USA).

3. Methods

3.1. Sample Preparation

Three etched foils overmolded by two different biopolymers resulted in six combinations (Table 3). Considering the four different surface treatments studied in this research and the corresponding pristine samples, there are 30 cases and 6 additional TPU-laminated cases. For each case, three samples were prepared to ensure repeatability and reproducibility.

Table 3. Sample layers.

Layer 1. Etched Polyimide Foil	Layer 2. Biopolymer
Upisel-N SR1220	PLA
Pyralux FR9120R	PHB
Shengyi SF305R	

An Engel 80T injection molding machine (Schwertberg, Austria) was used to make the overmolded samples. It was performed by fixing the PI flexible foil into the mold, followed by injecting the molten polymer over the foil. Before overmolding, the PLA and PHB pellets were dried for 24 h at 60 °C in a FarrgTech dryer (Vienna, Austria) to remove the moisture, preventing bubbles and/or air traps.

To conduct the experiment, the etched PI foils were cut into rectangles with dimensions of 40 × 300 mm^2, fitting in the mold. A rectangular aluminum mold with dimensions of 150 × 40 × 1.5 mm^3 was selected. The PI foils stick out of the mold to be able to perform the peel tests. The process steps are shown in Figure 1.

To achieve a high-quality sample, the injection molding process parameters, such as melting temperature, pressure, speed, and mold temperature, should be optimized for PLA and PHB. The parameter optimization is explained in detail in another study [26]. After adjusting the parameters, the pellets were poured into the hopper. At temperatures beyond the melting point (Table 1), the biopolymer melts and flows in the barrel by the injection screw. After the desired pressure is achieved, the molten biopolymer is injected into the

mold cavity and flows over the inserted PI foil. After solidifying, the mold is opened, and the overmolded foil is removed from the mold (Figure 1).

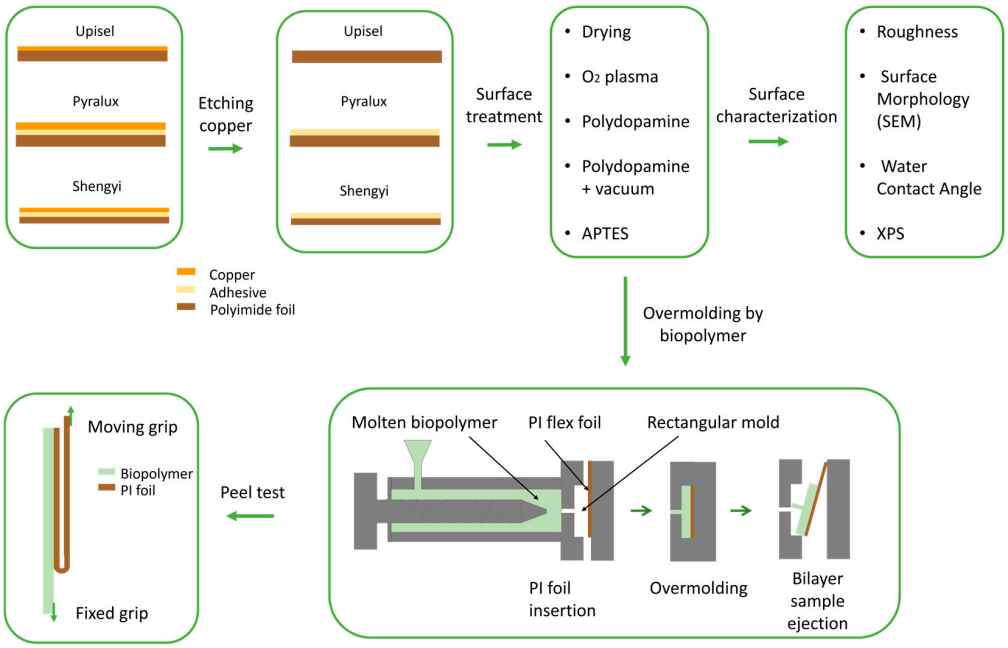

Figure 1. Schematic overview of sample fabrication using injection molding technology [26].

3.2. Surface Modifications

Five treatment methods were employed on three foils, including the following:

1. drying in an oven at 120 °C,
2. deposition of PDA,
3. deposition of PDA followed by thermal treatment at 50 °C in vacuum,
4. mild oxygen plasma,
5. surface modification with APTES.

In addition to these treatments, a TPU film was laminated on the PI foil as an adhesive tie layer. Overall, five different approaches were used to investigate the effectiveness of each in bonding two dissimilar polymers. Note that the surface treatments were conducted on the same day as the overmolding.

3.2.1. Drying

Prior to being placed in the mold, the foils were dried at 120 °C for 3 h in a FarrgTech oven (Vienna, Austria) to remove all moisture and volatile contaminants.

3.2.2. PDA Coating

The PDA modification is performed as described by Lee et al. in 2007 [27]. A 1500 mL 10 mM TRIS buffer solution is prepared and adjusted to pH 8.5 with 0.1 M HCl. Next, the substrates are inserted into this solution. Then, 3 g of dopamine. HCl is added. The mixture is kept in ambient air for 24 h. Finally, the modified samples are removed from the solution and rinsed with DI water.

3.2.3. PDA Coating with Thermal Treatment in Vacuum

This modification follows the same procedure as Section 3.2.2, but includes an additional thermal treatment step at 50 °C in a vacuum oven [25].

3.2.4. Plasma Activation

The PICO-Diener electronic GmbH & Co. KG system, Ebhausen, Germany, was used for this purpose. The PI foils were exposed to O_2 gas (0.8 mbar) plasma for 2 min. The power and frequency applied were 190 W and 40 kHz, respectively.

3.2.5. APTES Solution

Treatment of the PI surface with an APTES solution leads to the introduction of amino groups on the PI surface. The APTES solution was prepared by adding APTES (1 v%) to DI water and stirring for 1 min. Next, the PI foils were introduced in the APTES solution for 15 min, followed by a double rinse step in ethanol for 4 min. After drying with a N_2 gun, the samples were finally placed in an oven at 120 °C for 10 min.

3.2.6. TPU Lamination

The TPU tie layer is typically used in the textile industry as an adhesive glue activated by heat. A layer of TPU was laminated on the PI foil using a Lauffer RLKV 25 vacuum laminating press, Horb am Neckar, Germany. The lamination pressure and temperature profile are illustrated in Figure 2.

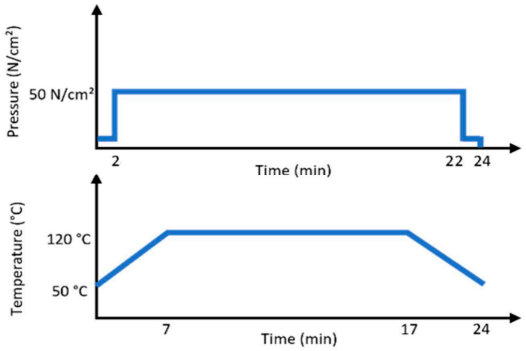

Figure 2. Pressure (**top**) and temperature (**bottom**) profile of the lamination process.

3.3. Surface Characterization

3.3.1. Static Water Contact Angle

The wettability of the PI foil surfaces before and after treatment was measured with a water contact angle (WCA) goniometer (EasyDrop, Krüss, Hamburg, Germany), using a 2 µL of distilled water droplet. For each (modified) foil, five measurements were performed at random spots. The angle was calculated by the fitting software of the goniometer using the circular fitting mode within 5–10 s after drop deposition.

3.3.2. Scanning Electron Microscopy

SEM analysis was performed to observe the loci of failure after peeling off the layers. Prior to analysis, the samples were coated with a thin gold layer (thickness of circa 20 nm) using a sputter coater (SPI, PA, USA). A JEOL JSM-5600 SEM (JEOL, Tokyo, Japan) apparatus equipped with a secondary electron detector was used for SEM imaging. An acceleration voltage of 5 kV was applied. The secondary electron images of the surface microroughness were obtained using a FEG SEM JEOL-7000F (JEOL, Japan). Prior to analyses, the samples were coated with a thin gold layer as described above. An acceleration voltage of 5 kV was applied.

3.3.3. Attenuated Total Reflection Fourier Transformed Infrared Spectroscopy (ATR-FTIR)

A Bruker Tensor 27 spectrometer equipped with a single reflection attenuated total reflectance accessory (MIRacle, Pike technology, WI, USA) was used to perform FTIR

analysis on the foils before and after modification, using a germanium crystal as the internal reflection element. All spectra were acquired using a mercury cadmium telluride (MCT) detector (liquid N_2 cooled) in the spectral region of 4000–700 cm^{-1}, and 64 scans with a resolution of 4 cm^{-1} were made for each sample.

3.3.4. Optical Profilometry

The root mean square roughness (R_{RMS}) values of the etched PI foils, before and after the surface modifications, were measured using a Wyko NT3300 optical profilometer (Veeco Instruments Inc., NY, USA). The white light vertical scanning interferometry (VSI) mode was selected. Surface scans were performed over a 228 × 300 μm^2 area. The R_{RMS} values were calculated using the integrated Vision software, Bruker, MA, USA. Three measurements are performed in three different areas at random locations.

3.3.5. X-Ray Photoelectron Spectroscopy

The surface chemical composition of the PI foils before and after treatment was assessed by XPS analysis. Measurements were conducted using a PHI Versaprobe II spectrometer (Physical Electronics, Japan) equipped with a monochromatic Al K_α X-ray source (hν = 1486.6 eV) operating at 25 W and possessing a beam size of 100 μm. The survey scans and high-resolution spectra were acquired with pass energies of 187.85 and 23.5 eV, respectively. All XPS measurements were conducted in a vacuum of at least 10^{-6} Pa with an angle of 45° between the sample surface and the analyzer. Four randomly selected points on each sample surface were analyzed to ensure representative results. Survey scans were processed using Multipak software (v 9.6), and Shirley backgrounds were applied to determine the sample elemental compositions. Multipak software was also used for curve-fitting of the high-resolution C1s peaks. To calibrate the energy scale, the C-C/C-H peak within the C1s spectrum at 285.0 eV was used as a reference. The high-resolution XPS peaks were then deconvoluted using Gaussian−Lorentzian peak shapes with a 1.4 eV limitation of the full width at half maximum (FWHM). In general, the depth of information for this surface analysis method was 5–10 nm for polymers.

3.3.6. Peel Test

The peel test is one of the most popular mechanical techniques for measuring the adhesive strength between two layers. In this study, the 180-degree peel test was performed. The overmolded samples (Section 3.1) were cut to a 30 mm width to avoid any edge effect. The end of the biopolymer (rigid layer) was fixed to the fixed grip, and the unbonded end of the PI foil (flexible layer) was fixed to the moving grip, as shown in Figure 3.

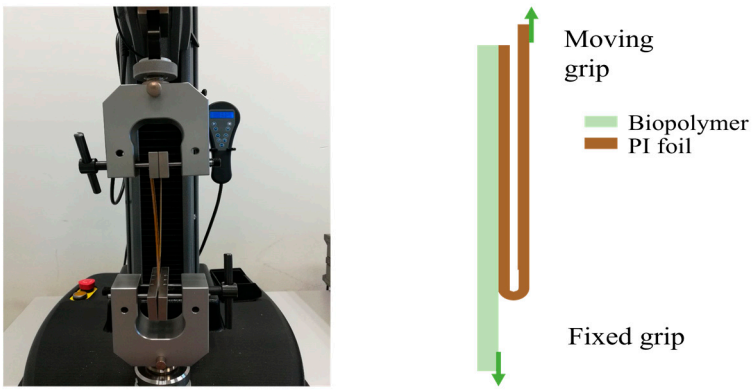

Figure 3. 180-peel test setup and schematic [26].

The Instron 5543 universal testing machine (MA, USA) equipped with a 500 N load cell was used to measure the peel strength at a crosshead speed of 10 mm/min. The peel strength (expressed in N/mm) was determined by calculating the average force divided by the sample width (30 mm).

3.4. Statistical Analysis

To statistically compare the results of our study, analysis methods such as the *t*-test and ANOVA (one-sided) were employed. The analysis was performed to determine if there is a significant difference between the means with one or more groups of (surface) foils. By applying these tests, we were able to quantitatively assess the impact of our experimental conditions on WCA values, atomic concentrations from XPS, roughness (R_{RMS}), and peel test results.

The results provided us with a *p*-value indicating the probability that the observed differences between the group means occurred by random chance. A *p*-value of less than 0.05 was considered statistically significant.

4. Results and Discussion

4.1. Introduction

The aim of the surface modifications is to chemically bond the overmolded PLA and PHB to the surfaces of the copper-etched foils (pristine foils) by several modification methods. This potentially leads to an increased adhesion towards overmolded biopolymers. PLA and PHB contain ester bonds as a linkage between the monomers (Figure 4). The end groups of the PLA and PHB contain carboxylic acid groups. In the presence of water at elevated temperatures, the ester groups of PLA and PHB can hydrolyse and result in additional carboxylic ester groups. Both primary amine and hydroxyl-containing molecules can react with these carboxylic groups to form amide linkages between modified surfaces and overmolded PLA at the interface [28]. It must be mentioned that amine groups are better nucleophiles compared to hydroxyl groups. The PDA coating (including vacuum-treated) contains primary amines and catechol groups [28], the APTES modified surface contains a primary amine, and the O_2 plasma-treated surfaces contain hydroxyl groups. It is obvious that other chemical and physical interactions (e.g., hydrogen bridges) can be formed at the interface of the modified surfaces and the overmolded PLA or PHB.

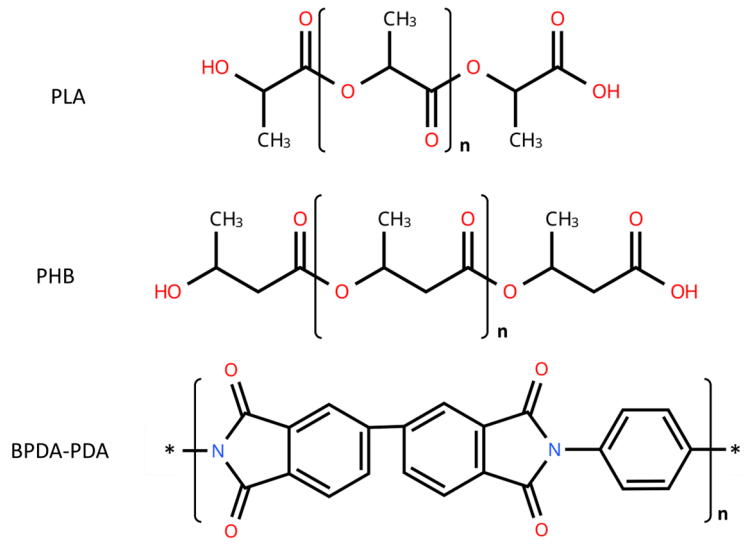

Figure 4. Chemical structure of PLA, PHB, and BPDA-PDA (The * indicates the linkage points to neighboring units in the polymer chain).

In the results and discussion part, ATR-IR is used to determine the chemical polymer composition of the adhesives or PI on top of the PI foils after Cu etching in Section 4.2. Next, the non-treated and modified surfaces of the etched polymer foils are characterized in terms of surface composition and surface morphology in Section 4.3. In the final section, the influence on the adhesive strength toward overmolded PLA and PHB is evaluated and compared with the addition of a TPU layer on the etched foils prior to overmolding.

4.2. Infrared Analyses of the Pristine Cu Etched Surfaces

Infrared spectroscopy is performed on all pristine samples to examine the chemical composition after etching the Cu. The infrared spectra are provided in Figures S1–S3. Because these foils are commercial products, the exact chemical composition of the top layer on the foils is very ill-defined. Nevertheless, it is possible to extract the main chemical building blocks into the adhesive layers of PI in the top layers.

The Upisel foil contains no adhesive layer. Therefore, the top layer after Cu etching is polyimide. The polyimide in Upisel foil consists of BPDA-PDA (poly(biphenyl dianhydride-p-phenylenediamine)). The chemical structure of this PI is illustrated in Figure 4. However, a top layer (2–3 μm) of similar PI with lower Tg is present to enable the lamination of Cu sheets onto this PI foil during production. The infrared spectrum of Upisel is shown in Figure S1. Characteristic peaks for BPDA-PDA are observed, such as imide I peaks (3074 cm^{-1} (C-H str), 1774 cm^{-1} (C=O sym str) and 1709 cm^{-1} (C=O asym str)), 1504 cm^{-1} (aromatic C=C str), imide II peak at 1376 cm^{-1} (C-N str), imide III peaks (1113 cm^{-1} and 1081 cm^{-1} (C-H bends)), and the imide IV peak at 736 cm^{-1} (C=O bend) [29–31].

The Pyralux foil contains an acrylic adhesive on top. The infrared spectrum is displayed in Figure S2. Clear peaks from an acrylic polymer are observed at 2961 cm^{-1} (C-H asym str from -CH_3), 2957 cm^{-1} (C-H asym str from -CH_3), 2874 cm^{-1} (C-H sym or asym str from -CH2- or -CH3), 1725 cm^{-1} (C=O sym str), 1447 cm^{-1} (C-H bend), and 1164 cm^{-1} (C-O-C str). Furthermore, a sharp small peak at 2242 cm^{-1} indicates the presence of a nitrile group (C≡N str), possibly due to the presence of a small amount of PAN (polyacrylonitrile) in the acrylic adhesive [32,33]. Furthermore, a peak at 1615 cm^{-1} (C=N str) can be assigned to the thermal cyclization of PAN, probably during the copper lamination in the fabrication process [34]. Finally, the presence of nitrogen in the XPS analysis also supports this.

The ShengYi foil is composed of a PI foil with an epoxy layer on top. The infrared spectrum in Figure S3 shows that it contains bisphenol A and glycidyl units. The so-called DGEBA type of epoxy resins [35–37]. The broad peak between 3200 and 3600 cm^{-1} can be assigned to O-H and N-H str. The methyl groups on the bisphenol A are visible through the C-H asym str and C-H sym str at 2963 cm^{-1} and 2880 cm^{-1}, respectively [38]. The other peaks in this area can be attributed to C-H asym str (2927 cm^{-1}) and C-H sym str (2840 cm^{-1}) from -CH_2- units. The C-H bend vibrations from show bands at 1455 cm^{-1} (twisting modes of -CH_2- groups and O-H bend) and 1296 cm^{-1} (C-H twisting and rocking). The aromatic C=C str band at 1505 and 1598 cm^{-1} is typical for bisphenol A, together with other peaks at 1238 cm^{-1} (aromatic C-O-C str), 1182 cm^{-1} (C-C str of the bridge carbons between two *para*-phenyl groups), and 827 cm^{-1} (aromatic C-H out of plane vibration) [35]. Furthermore, a small peak at 915 cm^{-1} (C-O str, ring vibration) can be assigned to unreacted epoxy groups [39]. Due to the presence of nitrogen in the XPS analysis (See Section 4.3.2), it is likely that organic molecules containing multiple nitrogen functionalities are present in this epoxy polymer. However, the nitrogen surface concentration obtained with XPS is quite small (1.3 at. %), so it is also possible that polyols are used as a reagent for epoxy polymer formation.

4.3. Surface Characterization of the Surface Modifications

4.3.1. Roughness, Surface Morphology, and Water Contact Angle

The roughness values, obtained from measurements with an optical profilometer, for each foil before and after the surface modifications are displayed in Table 4. To test if there were significant changes after or between the modifications in terms of roughness, a one-sided ANOVA test on the R_{RMS} values was run for each foil type. The result is that within each foil group, there is no significant difference ($p < 0.05$) between the modifications, including the pristine foil.

Table 4. Average values ± standard deviation (n = 9) of R_{RMS} (nm) before and after modification of the three foils.

PI Foil	Upisel	Pyralux	Shengyi
Pristine	203 ± 5	334 ± 34	304 ± 4
Plasma	206 ± 5	339 ± 32	302 ± 4
PDA	213 ± 6	327 ± 8	315 ± 12
PDA + Vacuum	204 ± 7	340 ± 25	307 ± 7
APTES	207 ± 5	331 ± 29	306 ± 5

Not only are the roughness values obtained with an optical profilometer important, but the surface microstructure of the foils after copper etching also shows important features on a (sub)micron scale. In Figure 5, FEG SEM images of the Upisel, Shengyi, and Pyralux after Cu etching (i.e., pristine surfaces prior to modification) are shown.

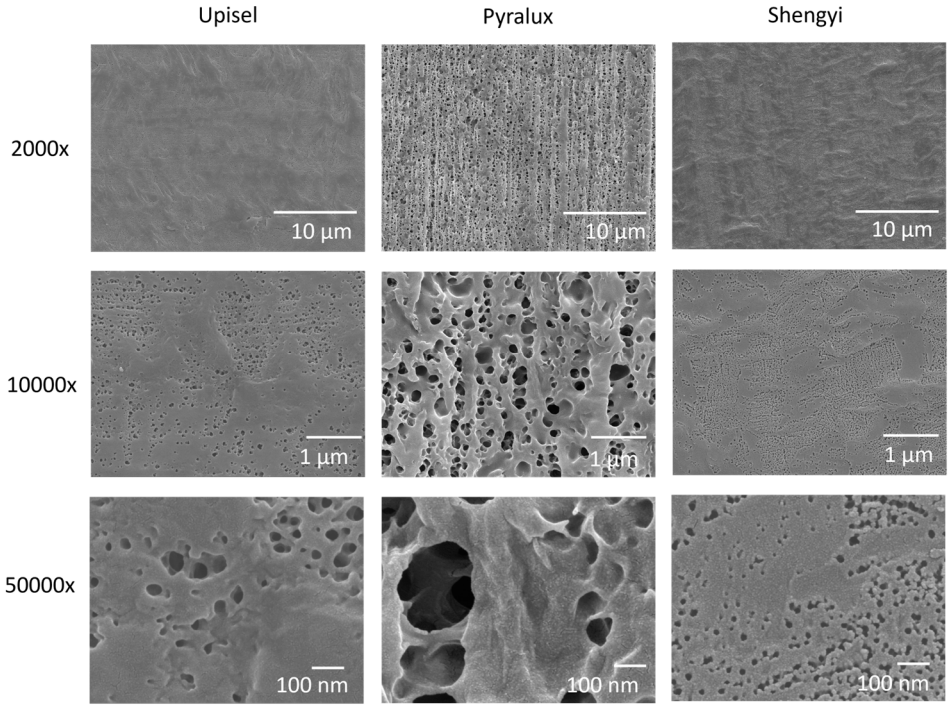

Figure 5. FEG SEM images of the Upisel, Shengyi, and Pyralux after Cu etching (i.e., pristine surfaces prior to modification).

Concerning the roughness of the pristine foils, it is important to mention that the production of all the PI-Cu foils contains a hot lamination step of the Cu foil onto the PI foils. This implies that the surface (micro)structures of the Cu foil are imprinted into the lower T_g PI top layer (in case of Upisel) or adhesive layer (in case of Pyralux and ShengYi) since the high-temperature vacuum laminations are performed above the glass

transition temperature or melting temperature of the PI or adhesive layers. Therefore, the surface microstructures after Cu etching depend on the microstructures present at the Cu foils. All the PI-Cu foils used in this work are produced using RA (rolled annealed Cu foils, typical for these flexible Cu-PI foils. The main reason for using the RA copper is the improved mechanical properties required for flexible applications [40]. The RA process introduces micrograins (also on the surface) due to the recrystallization of the Cu after thermal annealing. After this annealing process, a subsequent accumulative rolled (ARB) bonding process results in the presence of ultrafine grains (UFG). Depending on the number of ARB and thermal annealing cycles, the grain size can be reduced to submicron levels [40].

On the other hand, the Cu etchant solution used here to remove the Cu could also chemically attack the polymer layers (PI or adhesive layers), leading to (micro)porous structures. This depends on the chemical stability of the PI or adhesives against the etchant. To investigate this, the etched Cu samples (Pyralux and Shengyi) were exposed to an additional number of etching cycles (16 and 18 cycles). Note that the number of cycles needed to completely etch the Cu for these substrates was 14 cycles. The roughness and morphology did not change after increasing the etching cycles. This leads to the conclusion that the origin of the microstructure and roughness is due to the lamination/imprinting process during production of these foils as described above.

The surface microstructure of the pristine foils is shown in Figure 5, and the modified foils are analyzed with FEG SEM. The images of the modified PDA and PDA + Vacuum can be found in Figures S5–S8. On the pristine Upisel sample, regions with small (interconnected) pores with a diameter between 25 and 50 nm can be observed. The pores originate from chemical etching or from the imprinting of the Cu grain structure during the lamination step in the manufacturing process, as discussed above. The pristine Pyralux foils show a homogeneous porous surface structure. The pores are interconnected and have a diameter between 0.2 and 1 μm.

The pristine ShengYi foil contains two different areas. The first area shows a grain-sized area (diameter of 25–100 nm) without pores. The other area contains a porous structure but is still constructed of the same grains. The outcome of the surface microstructure analyses also matches the RMS values of the pristine foils (see Table 4). The lowest RMS value is found for the Upisel, followed by Pyralux and ShengYi.

After O_2 plasma and APTES treatment, there is no clear difference in the topography noticed between the corresponding SEM images for all foils. The same trend is observed for the R_{RMS} values of the three pristine foils versus plasma and APTES treatment, as there is no significant difference in the RRMS values before and after these modifications (see Table 4).

As already described in the literature [41–43], the PDA coating consists of a thin continuous layer originating from the adsorption of (poly)dopamine polymerization in solution. Next to that, larger coagulated particles (up to 150 nm in diameter) are deposited on the polymer surfaces. This can be attributed to particle formation and aggregation in solution, followed by adsorption on the surface at longer deposition times (after 10 min) [41]. It must be mentioned that the thickness of the PDA film and the density of PDA aggregates are influenced by the type of the target surface [44]. In this work, these aggregates are observed together with (single) grape or round particles (maximum diameter around 50 nm) deposited on the surface and inside of the pores on the FEG SEM micrographs (see Figures S5–S8).

The WCA results before and after the modifications are displayed in Figure 6. In general, the contact angle depends on the outermost chemical surface composition and the surface roughness in the case of non-absorbing surfaces [45]. This means that if the surface R_{RMS} roughness values do not change significantly before and after modification,

the difference between the WCA values before and after treatment can be mainly ascribed to chemical changes in the outermost surface. From the quantitative roughness analyses (see above Section 4.3.1), it is clear that the R_{RMS} values do not change significantly after modification. Therefore, the significant changes in WCA after the modifications can be attributed to chemical changes in the outermost surface, assuming that no absorption of the water takes place in the timeframe (5–10 s) of the WCA analyses.

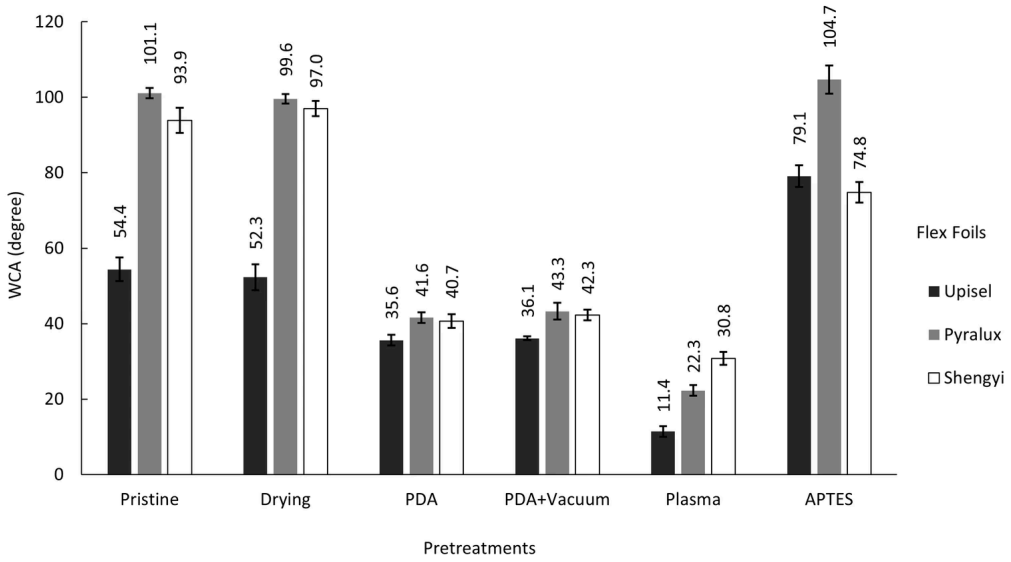

Figure 6. Water contact angles for pristine and treated PI foils. The reported values are the average value out of five measurements. The error bars represent the standard deviation.

An average contact angle of 54.4 ± 3.1° was obtained for the pristine Upisel foil. However, pristine Pyralux and Shengyi foils show much higher average contact angles (101.1 ± 1.4° and 93.9 ± 3.3°, respectively), indicating hydrophobicity. As mentioned before (Section 2), the top layer of the Pyralux and Shengyi foils is an acrylic and epoxy adhesive, respectively. Through XPS analyses (Section 4.3.2), it became clear that the Upisel and the Pyralux foils show CrO_x on their surface. The evaporation of a thin layer of Cr on the Cu foil (thickness of a few nm) is a common technique to improve the adhesion towards polymer foils. Nevertheless, it is contradictory that the WCA of the Upisel foil is 54.4 ± 3.1° and the Pyralux foil is 101 ± 1.4°. The only valid conclusion is that the Pyralux foil surface is contaminated [46]. Finally, the hydrophobic surface of the Shengyi foil (WCA = 93.9°) also suggests contamination since this result is not expected for an epoxy-based material. Probably, this contamination could be attributed to hydrocarbon contamination since the oxygen plasma results in a decrease in the WCA to 36.3° combined with a decrease in the carbon surface concentration determined by XPS (see Section 4.3.2).

The APTES modification of the Upisel foil results in an increase in the WCA from 54.4° to 79.1°. In contrast, a decrease in the WCA from 93.9° to 74.8° is observed for Shengyi. Both of these foils are hydrophilic after APTES treatment and show a contact angle of around 75–80°. There is no significant difference ($p < 0.05$) in WCA after APTES treatment of the Pyralux foil, and the surface remains hydrophobic.

The WCA is reduced for all three foils after oxygen plasma treatment. There is a significant difference ($p < 0.05$) between WCA values before and after plasma treatment. The lowest value was achieved for the plasma-treated Upisel foil, reaching a WCA value of 11.4°. Plasma treatment with O_2 gas introduces oxygen-containing functional groups such as carboxyl (-O-C=O), carbonyl (-C=O), and hydroxyl (-C-OH) on polymer surfaces. Therefore, the contact angle of polymer surfaces is expected to decrease after oxygen plasma treatment [47].

After the PDA coating, a significant decrease in the contact angle was obtained for all three foils. This could be attributed to the introduction of catechol, hydroquinone, and several types of amine groups on the PI surface [48]. In this case, the WCA of the three foils lies between 30° and 40°.

A comparison of WCA values and images before and after the performed surface modifications is shown in Figure 7 for the Upisel foil as an example.

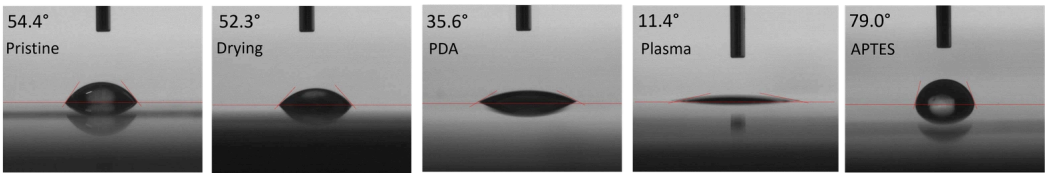

Figure 7. Images of WCA measurements for different surface treatments on Upisel foil.

It should be noted that plasma-treated samples are subject to hydrophobic recovery (aging) over time due to the tendency of polymer segments containing hydrophobic groups to reorient from the bulk to the surface of the polymer [49]. The foils were therefore overmolded within 5 h after plasma treatment. As such, the WCA for all three foils was remeasured 5 h after plasma treatment, resulting in WCA values of 13.4°, 55.1°, and 62.3° for Upisel, Pyralux, and Shengyi, respectively. These values suggest that the foil's surfaces still remain hydrophilic before the overmolding step.

4.3.2. Evaluation of the Surface Chemical Compositions (XPS)

XPS analysis was used to evaluate and confirm the performed surface modifications. The average elemental composition of the analyzed surfaces is summarized in Tables 5–7 for the three PI foils.

Table 5. Elemental composition of Upisel foil surfaces with various treatments. Each value is presented as an average value (n = 4) ± standard deviation. * DL stands for detection limit.

Upisel Foil	C (at. %)	O (at. %)	N (at. %)	Si (at. %)	Cr (at. %)
Pristine	38.9 ± 1.0	45.0 ± 0.8	3.7 ± 1.4	2.4 ± 0.8	9.6 ± 0.8
PDA	72.4 ±0.7	20.1 ± 0.5	7.3 ± 0.5	<DL *	<DL
PDA + Vacuum	70.0 ± 0.7	21.6 ± 0.4	8.2 ± 0.5	<DL	<DL
Plasma	36.5 ± 1.2	47.1 ± 0.6	4.6 ± 1.5	3.3 ± 0.8	8.5 ± 1.1
APTES	34.9 ± 0.8	43.4 ± 1.8	5.0 ± 0.7	5.6 ± 0.6	11.7 ± 2.6

Table 6. Elemental composition of Pyralux foil surfaces with various treatments. Each value is presented as an average value (n = 4) ± standard deviation. * DL stands for detection limit.

Pyralux Foil (Acrylic)	C (at. %)	O (at. %)	N (at. %)	Si (at. %)	Cr (at. %)	S (at. %)
Pristine	48.7 ± 2.8	40.3 ± 1.5	4.0 ± 0.8	<DL *	4.9 ± 0.4	2.0 ± 0.5
PDA	69.3 ± 0.7	23.0 ± 0.4	7.4 ± 0.6	<DL	<DL	<DL
PDA + Vacuum	72.3 ± 0.7	21.1 ± 0.5	6.5 ± 0.4	<DL	<DL	<DL
Plasma	37.5 ± 1.4	50.0 ± 0.4	3.4 ± 0.4	<DL	6.9 ± 1.1	2.2 ± 0.3
APTES	50.4 ± 0.4	36.8 ± 0.6	5.3 ± 1.0	1.8 ± 0.6	4.7 ± 0.4	0.9 ± 0.3

Table 7. Elemental composition of Shengyi foil surfaces with various treatments. Each value is presented as an average value (n = 4) ± standard deviation. * DL stands for detection limit.

Shengyi Foil (Epoxy)	C (at. %)	O (at. %)	N (at. %)	Si (at. %)	S (at. %)
Pristine	76.1 ± 0.6	21.2 ± 1.0	1.3 ± 1.2	<DL *	0.6 ± 0.2
PDA	74.0 ± 0.4	19.4 ± 0.2	6.3 ± 0.3	<DL	0.1 ± 0.1
PDA + Vacuum	76.3 ± 0.4	18.3 ± 0.2	5.4 ± 0.2	<DL	<DL
Plasma	61.0 ± 0.6	34.5 ± 0.6	3.6 ± 1.0	<DL	0.6 ± 0.2
APTES	71.8 ± 2.4	22.5 ± 0.4	3.2 ± 2.3	1.8 ± 0.4	0.5 ± 0.4

In addition to carbon, oxygen, and nitrogen being part of the chemical structure of all three non-modified foil types, other elements such as chromium, silicon, and sulfur are also present on some of the pristine PI foils. Chromium originates from evaporated Cr on the backside of the Cu for Upisel and Pyralux. A thin layer (order of a few nanometers) of Cr is deposited prior to the PI-Cu clad laminate fabrication process and is beneficial for the adhesion between the Cu and the polymer foils. On the pristine samples, sulfur (Pyralux and Shengyi) and silicon (Upisel) are also observed in small concentrations. These elements are present in the (top) polymers. The presence of these elements in the bulk polymers is also confirmed by energy dispersive spectroscopy on all pristine foils. As a consequence, the presence of these elements in the XPS analyses can be assigned to the inherent composition of the adhesives (Pyralux and Shengyi) or the top layer of the PI (Upisel).

The curve-fitted C1s high-resolution spectra of the pristine and surface-treated PI foils are presented in Figure 8, revealing the chemical status of the carbon atoms at the surface. The table with relative individual contributions of the peaks after deconvolution and integration can be found in the supporting info (Table S1).

The pristine Upisel C1s deconvoluted spectrum shows the presence of C-C/C-H/C=C, C-N, and N-C=O peaks, which are typical for an aromatic polyimide. The contribution of the C-N peak is higher than expected. This could be attributed to additional C-O or C-N presence due to organic contamination, minor decomposition products from the Cu etching process, or incompletely cured BPDA-PDA. Finally, a small contribution of Si-C is also observed.

The Pyralux foil contains an adhesive layer composed of acrylic resin and polyacrylonitrile (smaller fraction), as concluded from the ATR-FTIR results. This is confirmed by the presence of C-C/C-H, C-O/C-N/C=N, **C**-O-C=O, and O-C=O peaks. The presence of nitrogen in the XPS analysis (see Table 5) can be attributed to polyacrylonitrile and thermal cyclization products (created during production (i.e., hot lamination of Cu foil on PI + adhesive foil) of polyacrylonitrile.

The Shengyi foil has an epoxy adhesive on top of the PI. The presence of a C-C/C-H and C-N/C-O peak confirms this.

To verify that the polydopamine is deposited on the surface, reference Si pieces were added to the same modification protocols as for the foils. Both PDA and PDA + Vacuum modifications on Si result in the addition of carbon, oxygen, and nitrogen on the samples' surface (see Table 8). However, in both cases, Si is also detected. The N/C ratio for PDA and PDA + Vac on Si is 0.12 in both cases. This is close to 0.125, the theoretical value for PDA. The O/C ratio cannot be used here as a comparison because there is an additional oxygen contribution from the top native SiOx layer on the modified Si pieces in the XPS analysis results.

Table 8. Elemental composition of the silicon sample as a reference treated with PDA and PDA + vacuum.

Si Reference	C (at. %)	O (at. %)	N (at. %)	Si (at. %)
PDA	63.1 ± 0.3	21.9 ± 0.2	7.6 ± 0.6	7.4 ± 0.6
PDA + Vacuum	59.9 ± 1.4	22.4 ± 0.4	7.3 ± 0.5	10.3 ± 1.1

As described in Section 4.3.2, the PDA forms a continuous homogeneous film with adsorbed PDA aggregates on top. Together with the presence of Si in the XPS spectra, this leads to the conclusion that the homogenous PDA film is thinner than the depth of information of XPS (5–10 nm) on the PDA modified Si pieces.

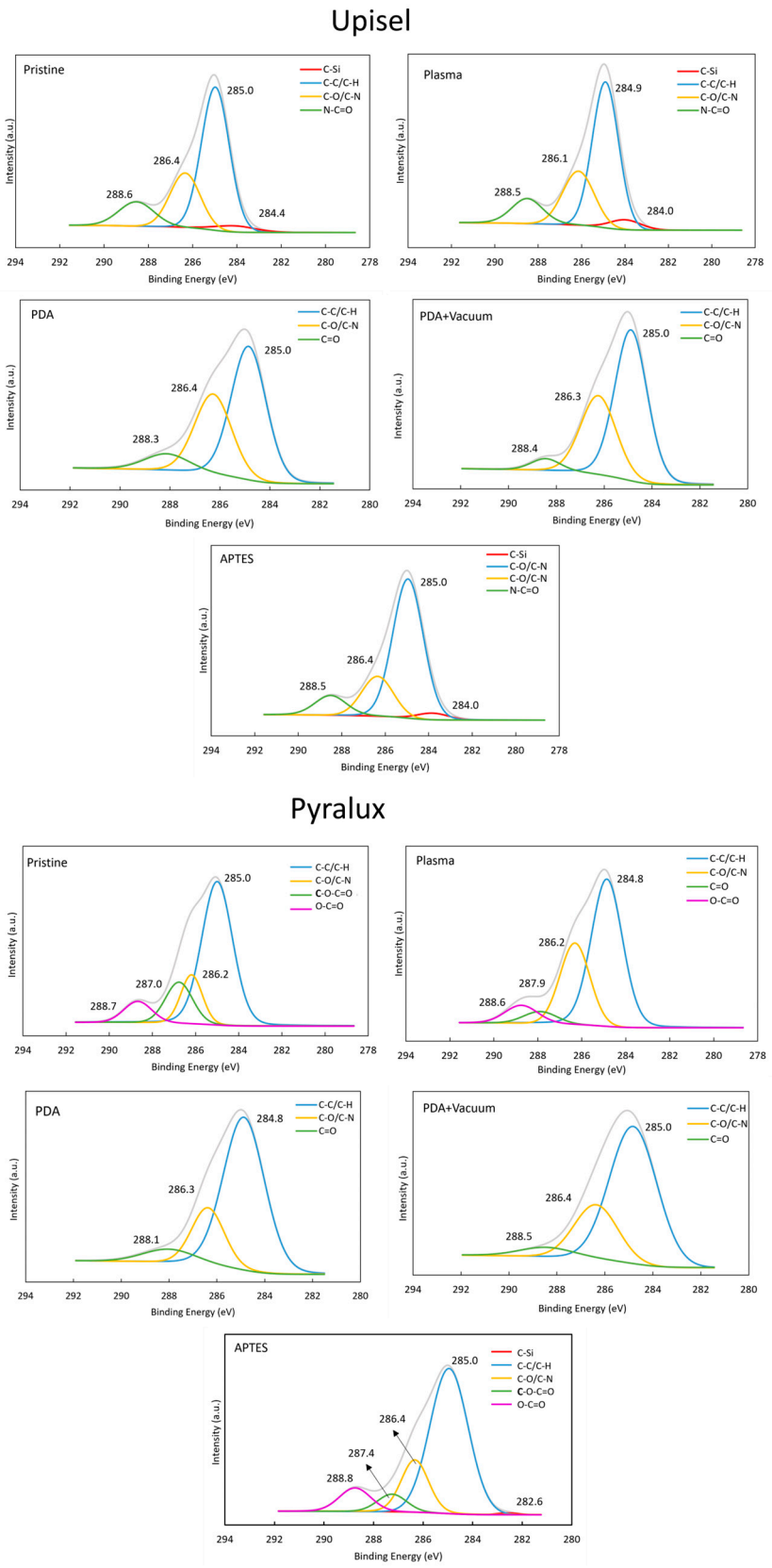

Figure 8. *Cont.*

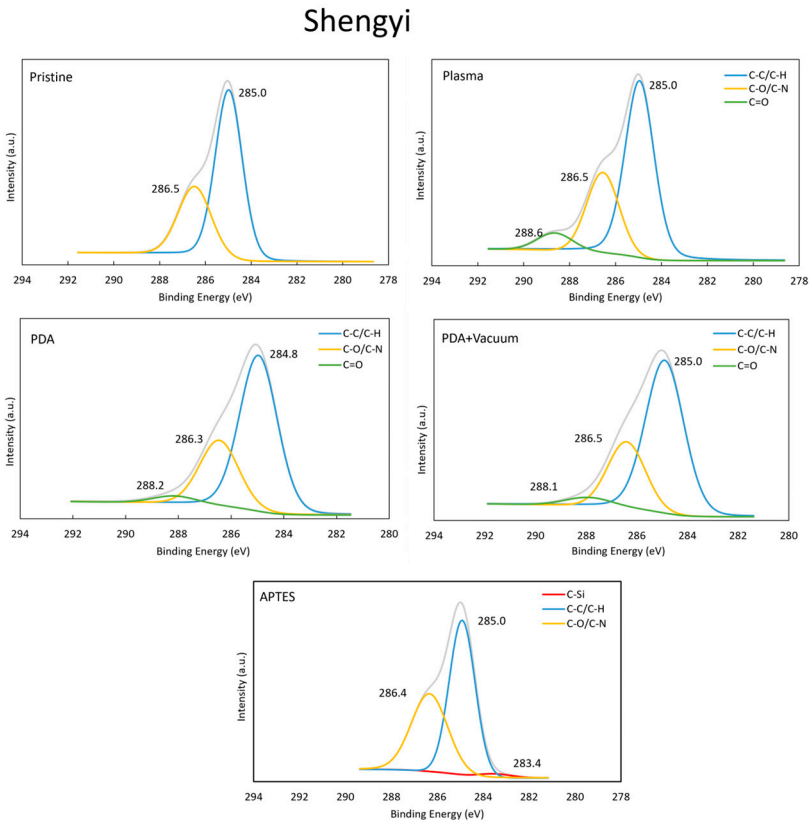

Figure 8. Deconvoluted high-resolution C1s spectra of the three foils before and after O_2 plasma, PDA, PDA with vacuum, and APTES modifications.

The polydopamine modification is characterized by a significant increase in N concentration on the surface for all foils. Since, in this work, the polydopamine homogeneous layers are thinner than the XPS depth of information of polymers (5–10 nm), the total XPS surface elemental composition contains contributions of both the polydopamine and the underlying polymer surface. As a consequence, the C/O/N ratio after PDA modification cannot be compared with the theoretical C/O/N ratio of polydopamine. However, due to the differences in the amount of the polydopamine aggregates on each foil substrate (See Figures S5–S8), the nitrogen increase after PDA modification can differ from foil to foil.

This is also reflected in the uniformity of the WCA values after PDA modification. All three foils show WCA values between 35° and 45°, independent of their initial WCA values. The relatively low standard deviations on each of the foils show that the PDA modifications are quite uniform on a large scale.

For all foils, the curve fittings of the high-resolution C1s spectra after PDA modification clearly show a change. However, due to the contribution of the underlying polymers, the changes and contributions (C-H/C-C, C-O, C-N, and C=O peaks) in these C1s spectra cannot be assigned to polydopamine exclusively. The high-resolution C1s spectra of PDA modified Si (see Figure S9) present in the same modification solution show good accordance with spectra in the literature [50].

The evaluation of the XPS data for Upisel and Pyralux after oxygen plasma treatment is not straightforward due to the presence of CrO_x on the surface of these foils, assuming the spontaneous oxidation of Cr to CrO_x under ambient conditions after Cu etching. The initial surface composition of both foils shows relatively lower amounts of carbon and the presence of nitrogen. These elements can be attributed to the underlying polymers (PI or acrylic adhesive) and/or hydrocarbon contamination. This means that the depth

of information is larger than the thickness of the Cr/CrO_x layer, or the distribution of the Cr/CrO_x layer is not uniform.

After oxygen plasma treatment of the Upisel foil, there is only a small reduction in carbon and a small increase in oxygen, revealing minor differences in the O/C atomic ratio (Table 9). This is also reflected in the fact that the high-resolution C1s spectra of the Upisel foil before and after plasma treatment are very similar [51,52]. However, in this case, the WCA is reduced from 54.4° to 11.4°. Next to the minor oxidation of the Upisel foil, this reduction could be ascribed to the removal of hydrocarbon surface contamination, a very small amount of introduced oxygen-containing groups on the polymer, and/or further Cr oxidation during plasma treatment. Note that there is a difference in depth of information between WCA and XPS if the polymer does not absorb water. The WCA depends on the interaction with the outermost surface layer, and the depth of information for XPS of polymers is 5–10 nm. This could also be the reason for this observation of the WCA decrease.

Table 9. O/C atomic ratio before and after oxygen plasma treatment.

PI Foil	Upisel	Pyralux	Shengyi
O/C before plasma	1.2	0.8	0.3
O/C after plasma	1.3	1.3	0.6

In contrast to the Upisel foil, Pyralux shows a larger reduction in carbon surface content and a larger increase in O surface content after plasma treatment. This is also evidenced by the increased O/C ratio after plasma treatment, as shown in Table 9. A closer look at the C1s detail spectra of the pristine Pyralux and the oxygen plasma-treated Pyralux (Figure 8) reveals that the relative number of C-C/C-H decreases after plasma treatment (from 61% to 53%) (Table S1). The surface oxidation is responsible for the large decrease in WCA from 101.1° to 22.3°. As the total Cr surface content is lower compared to the Upisel foil, the plasma treatment can cause more significant changes to this polymer surface. These changes could be attributed to the introduction of C-O bonds on the polymer after oxygen plasma treatment and/or the removal of hydrocarbon contamination. A relative increase in the C-O contribution can clearly be observed in the C1s deconvoluted spectra (Figure 8) and integrated values (Table S1) after plasma treatment. However, a slight decrease in the C=O and O-C=O peaks is also observed.

The Shengyi foil surface does not contain Cr/CrO_x on the surface. After O_2 plasma treatment, it shows a large increase in the O/C atomic ratio from 0.3 to 0.6 (Table 9). This can be ascribed to the introduction of additional C-O and C=O functional groups [47]. From the C1s high-resolution spectra (Figure 8), a new C=O peak is observed after plasma treatment, which is an indication of the carbon oxidation by the O_2 plasma. Quite unexpectedly, a significant increase in nitrogen concentration from 1.3 to 3.6 at. % is noticed (see Table 7).

The third surface modification is performed with APTES. Theoretically, this should introduce Si, N, and C on the modified surface. However, all pristine foils already contain carbon and nitrogen, while the Upisel foil also contains silicon on its pristine surface. To investigate if the surface was modified with APTES, only the Si and N contents are compared before and after modification. Carbon content is not ideal for comparison, as it can be disturbed by contributions of hydrocarbon contamination.

In the case of the Upisel foil, a significant increase in the Si concentration ($p < 0.05$) is observed after APTES modification. However, no significant increase in the N concentration is obtained. Comparing the deconvoluted high-resolution C1s spectra before and after treatment reveals a small but significant increase in the C-Si contribution. On the other hand, the WCA after modification increases by circa 25°. A possible explanation could be

the difference in depth of information between XPS and WCA. This means that the surface was modified. It cannot be confirmed that this modification is homogeneously distributed.

A clear increase in the Si concentration after APTES modification is obtained for the Pyralux foil, combined with a slight increase in the N concentration, with a low significance level ($p < 0.1$). The high-resolution C1s spectra reveal a small contribution (circa 1%) to the C-Si after modification. However, there is a very small change in the WCA after modification. This leads to the conclusion that there is a very low number of APTES present on the surface, and it is not homogeneously covering the surface.

A similar conclusion for the Upisel can be drawn for the Shengyi foil. On this particular sample, there is quite some variation in the measured N concentration as evidenced by the relatively large standard deviation (N at. %: 3.25 ± 2.33). This suggests that the APTES modification is not homogeneously distributed.

In review, the O_2 plasma, PDA, and PDA + Vacuum surface modifications demonstrated effective chemical changes, resulting in altered surface chemical properties. The APTES surface modifications could not be completely confirmed by the XPS results and are not uniform. However, for the Upisel and Shengyi foils, the APTES treatment resulted in severe differences in WCA (20–25°).

4.3.3. Surface Characterization Conclusion

After etching the Cu of all foils, the surfaces were modified with PDA, O_2 plasma, and APTES. The WCA and XPS analyses results before and after the modifications lead to the conclusions listed below.

PDA: A thin, uniform PDA layer is deposited on all three foils. However, the amount of polydopamine aggregates differs from foil to foil.

O_2 plasma: A decrease in hydrophilicity is observed for all foils due to the introduction of C-O and/or C=O functional groups on the surface, combined with the removal of the hydrocarbon contamination.

APTES: A limited number of APTES is deposited on the surface of the foils, leading to changes in WCA in the case of Upisel and Shengyi.

Both on the Upisel and Pyralux foils, a thin layer of CrO_x is present, originating from pretreatments of the Cu foil during fabrication. Unexpectedly, the initial Pyralux and Shengyi foils have WCA values above 90° (hydrophobic) despite the CrO_x and/or polymer-based adhesives on the surfaces. Nevertheless, after O_2 plasma treatment, a hydrophilic surface is obtained for all foils.

4.4. Adhesive Strength

4.4.1. Adhesive Strength Measurements

The measurement results of 36 combinations are displayed in Figure 9. An inset is included for the lower values. There are six combinations of PI foils and biopolymers named PI foil/biopolymer (Table 3). The pristine samples serve as a reference for all treatments.

For each modification and material combination, Table 10 provides an overview of the type of failure based on visual and SEM inspections after peeling.

Adhesive strength values of pristine Upisel and Pyralux foils towards PLA and PHB are very low (≤0.05 N/mm) and considered negligible. Some surface modifications only result in a marginal increase in peel strength (≤0.05 N/mm), but we do not discuss these here.

The Upisel foil with the lowest initial roughness value (205 ± 5 nm) shows a very small improvement after oxygen plasma treatment and a large improvement when TPU is applied as a hotmelt adhesive. For PLA and PHB, the results are 1.62 N/mm and 0.97 N/mm, respectively. Mashayeki investigated the influence of surface modifications (cleaning and drying, plasma, PDA, and chemical etching and roughening of a smooth PI

foil (order of nanometers) on the adhesive strength towards compression molded PLA [24]. These results are difficult to compare with the results from our study because there is a large difference in roughness values (nanometers versus hundreds of nanometers) after plasma treatment and PDA modification. Moreover, CrO_x is present on the surface of our Upisel foils. Mashayeki et al. only found a small increase in adhesive strength (up to 0.1 N/mm) when the surfaces are roughened by grinding, whether or not combined with PDA modification.

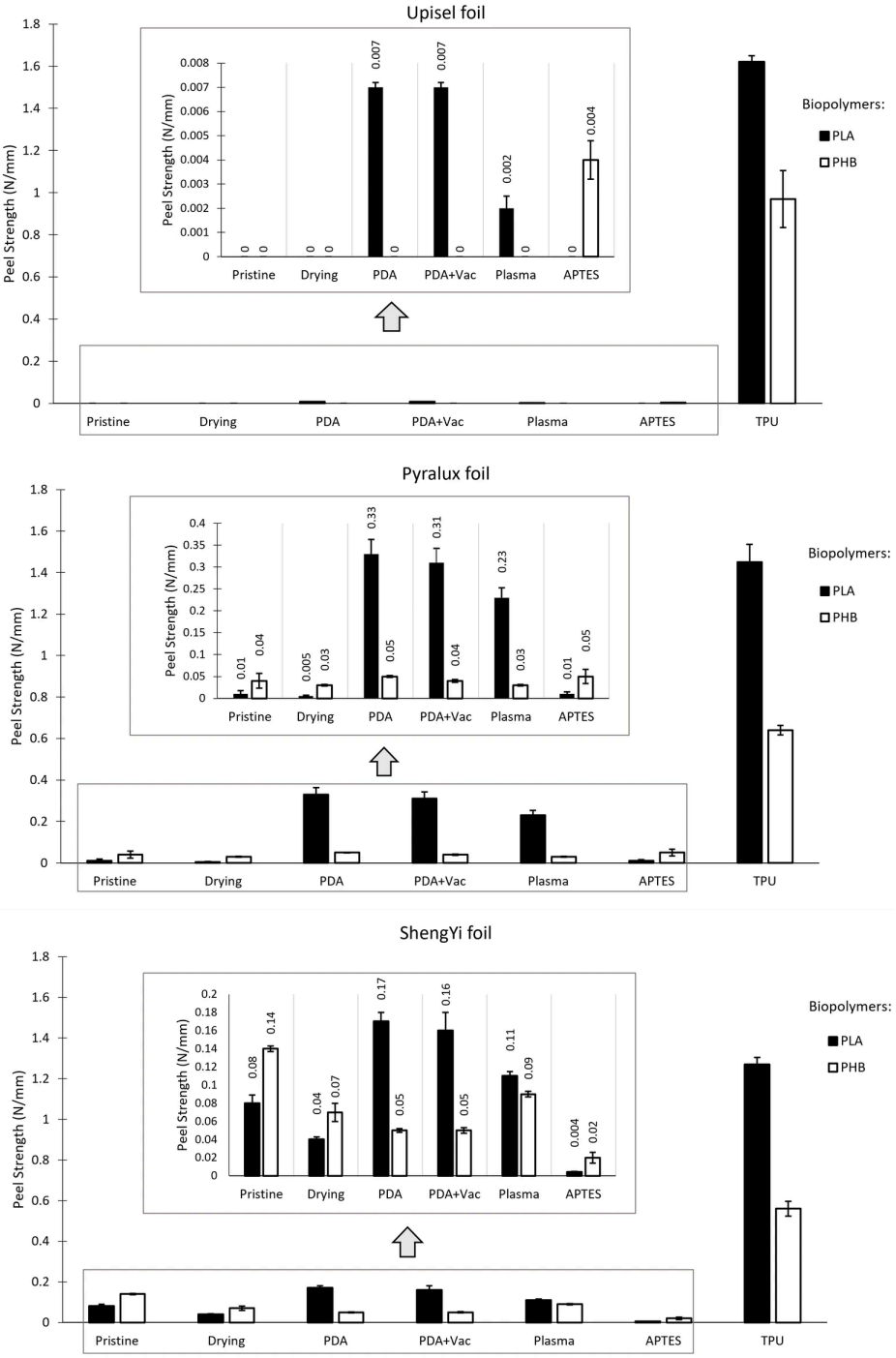

Figure 9. Average peel strength between PI foils and biopolymers (PLA or PHB) for different surface treatments. The error bars represent the standard deviation (n = 3).

Table 10. Overview of the failure type of all samples.

Sample	Upisel/PLA	Upisel/PHB	Pyralux/PLA	Pyralux/PHB	Shengyi/PLA	Shengyi/PHB
Pristine	Adhesive	Adhesive	Adhesive	Adhesive	Adhesive	Adhesive
Drying	Adhesive	Adhesive	Adhesive	Adhesive	Adhesive	Adhesive
PDA	Adhesive	Adhesive	Adhesive/ Cohesive	Adhesive	Adhesive/ Cohesive	Adhesive
PDA + Vacuum	Adhesive	Adhesive	Adhesive/ Cohesive	Adhesive	Adhesive/ Cohesive	Adhesive
O2 plasma	Adhesive	Adhesive	Adhesive/ Cohesive	Adhesive	Adhesive/ Cohesive	Adhesive
APTES	Adhesive	Adhesive	Adhesive	Adhesive	Adhesive	Adhesive
TPU	Cohesive	Cohesive	Cohesive	Cohesive	Cohesive	Cohesive

In contrast to the Upisel foil, an increase in the adhesive strength is observed after surface modification with PDA, PDA + VAC, and O_2 plasma treatment (from 0.01 N/mm to 0.33 and 0.31 N/mm, respectively) for Pyralux foil. Since the PDA fully covers the substrate surface (Section 4.3.2), this increase can be ascribed to the larger initial surface roughness of Pyralux versus Upisel.

The Shengyi foils do not contain a CrO_x layer on the surface, as can be seen from the XPS results (Table 7). Based on the information of the provider, an epoxy resin layer is present after Cu etching. The adhesive strength of the pristine samples toward overmolded PLA is 0.08 ± 0.09 N/mm.

A significant increase in peel strength is observed after modification of the Shengyi foil with PDA, PDA + VAC, and O_2 plasma to values of 0.16, 0.17, and 0.14 N/mm, respectively. These values are lower compared to the values obtained for Pyralux. Since the chemical surface composition is the same for PDA modification, this can partially be ascribed to the lower roughness of the Shengyi foils in the areas where adhesive failure is observed (see Table 9). In the case of oxygen plasma modification, it is difficult to compare due to both differences in roughness and surface composition (CrO_x on the Pyralux foils).

Finally, in contrast to what was described by Kafkopoulos et al. [25], an increased adhesive strength of molded PLA toward PDA vacuum-treated at 50 °C versus PDA was not observed for all foil types.

Compared to the peel strengths of the overmolded PLA with TPU laminate for Upisel, Pyralux, and Shengyi, the PHB shows lower values for all three foils. Both PLA and PHB with TPU show a complete cohesive failure within the TPU foil after peel tests in all cases. The lower peel strengths can be ascribed to the different parameters used for the overmolding process (including the cooling-down process) of PLA and PHB.

PHB spontaneously peels off when overmolding the pristine, O_2 plasma-treated, and PDA-modified Upisel foil. Only the APTES modification resulted in a negligible increase in the peel strength to 0.004 N/mm. This could possibly be ascribed to the increased contact angle value after APTES modification from 54.4° to 79.1° (see Figure 6).

Despite the large differences in WCA values of Pyralux before and after surface modifications with O_2 plasma and PDA, only minor differences (≤0.02 N/mm) in peel strength values are obtained after overmolding with PHB. Only a small difference in the WCA value after APTES modification is observed, leading to a peel strength of 0.05 N/mm after overmolding with PHB. These results suggest that contact angles around 20° and 100° do not lead to good adhesion towards overmolded PHB.

The only relevant observation is that for the Shengyi foil, the adhesive strength of the pristine foil is higher (0.14 N/mm) than after the surface modifications, except for the TPU hot melt adhesive. This means that the chemical surface composition of the epoxy resin itself is better matched to the PHB.

In conclusion, the chemical modification and drying methods described here do not result in an acceptable increase in the adhesive peel strength. A more precise and targeted modification to optimize the free surface energy of the foil surfaces is needed. This approach requires good determination or estimation of the surface free energy of the viscous PLA/PHB interacting with the foil surface during and after overmolding.

4.4.2. Loci of Failure

SEM analyses were conducted to determine the loci of failure between the two layers after separation at the end of the peel tests. This is achieved by performing SEM analyses on the PI side and PLA side, as shown in Figure 10. Looking at Table 9, there is a clear relationship between the obtained adhesive strength values (see Figure 7) and the failure mode. In general, low adhesive strength (from 0 to 0.1 N/mm) results in adhesive failure between the PI and biopolymer surfaces.

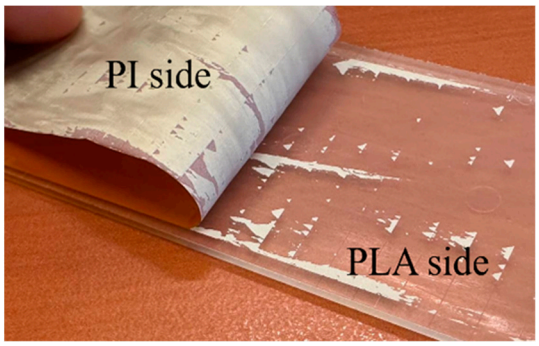

Figure 10. Plasma-treated Pyralux/PLA sample after peel test for SEM analysis.

An overview of SEM images of the Pyralux/PLA and Shengyi/PLA for pristine, plasma, PDA, and TPU cases is shown in Figure 11. A mixed cohesive and adhesive failure is observed in the case of Pyralux/PLA and Shengyi/PLA modified with PDA or O_2 plasma. In these cases, the cohesive failure is located in the acrylic (Pyralux) or epoxy (Shengyi) adhesive material. At those locations, the adhesive strength between the surface-modified PI and PLA is higher than the cohesive strength within the adhesive layers.

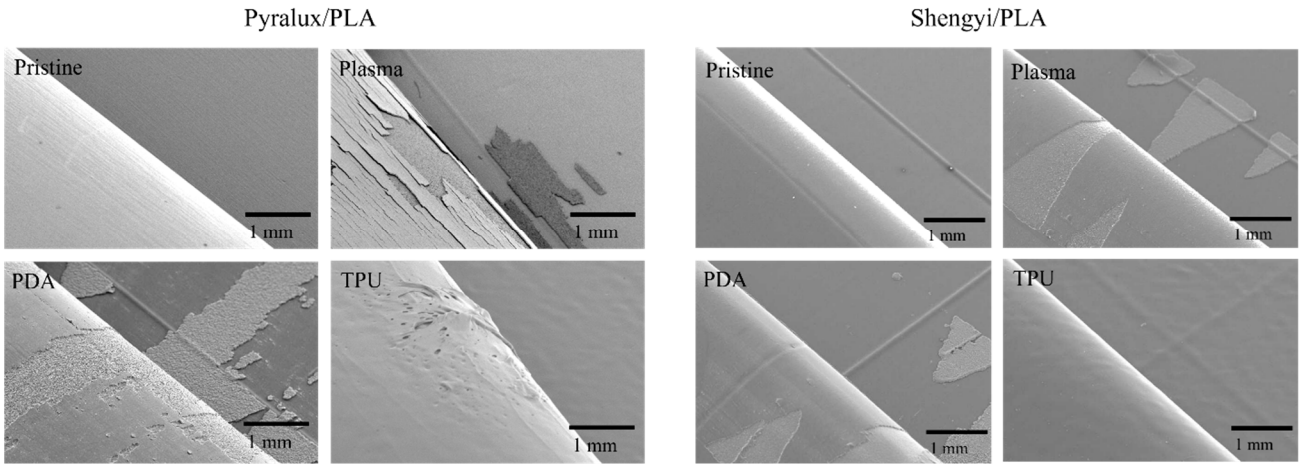

Figure 11. Overview of SEM images of Pyralux/PLA and Shengyi/PLA of four different cases.

Overall, the adhesive failure areas are larger compared to the cohesive failure areas. This could be attributed to incomplete wetting of the viscous PLA during overmolding, leading to areas where there is no physical contact between PLA and the modified surfaces. Important to note here is that the obtained peel strength values are quite low

(0.23–0.24 N/mm). Typically, cohesive failure within the epoxy and acrylic layers is unexpected. However, during overmolding, a short contact with hot viscous PLA (200 °C) followed by fast cooling can alter the properties of the adhesives. Figure 12 shows the cohesive failure that occurred within the acrylic adhesive for the plasma and PDA treated Pyralux/PLA sample.

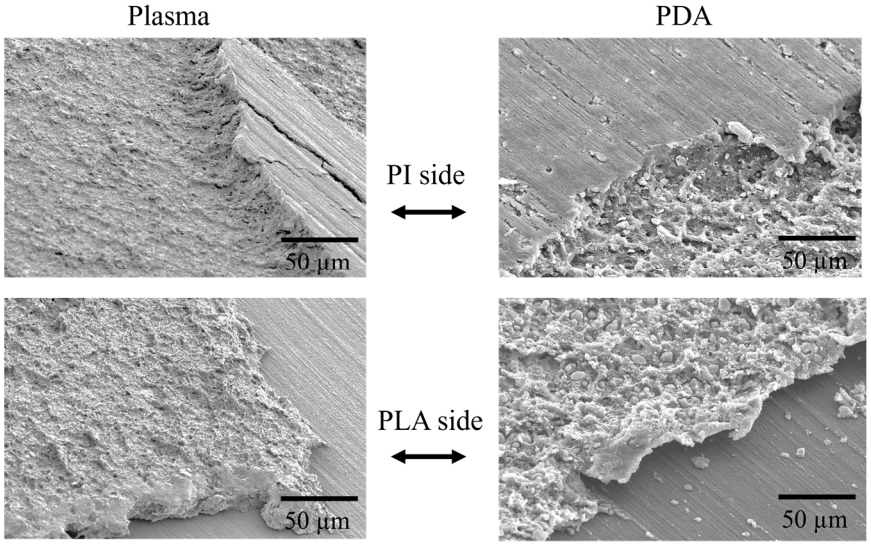

Figure 12. Cohesive failure within the acrylic adhesive layer after peeling off the PI and PLA.

Higher peel strength values are obtained when using TPU as a hot-melt adhesive on the foils. Here, a cohesive failure of the TPU material is observed (Figure 13). It is important to note that there is quite a variation in these values. In our opinion, this could probably be ascribed to the melting behavior of the TPU during overmolding with PLA at 200 °C. Consequently, the TPU material underwent a gradient of temperature exposure from top to bottom. Directly after injection, the TPU cools down quickly, leading to inhomogeneous material properties from the top to the bottom of the sample.

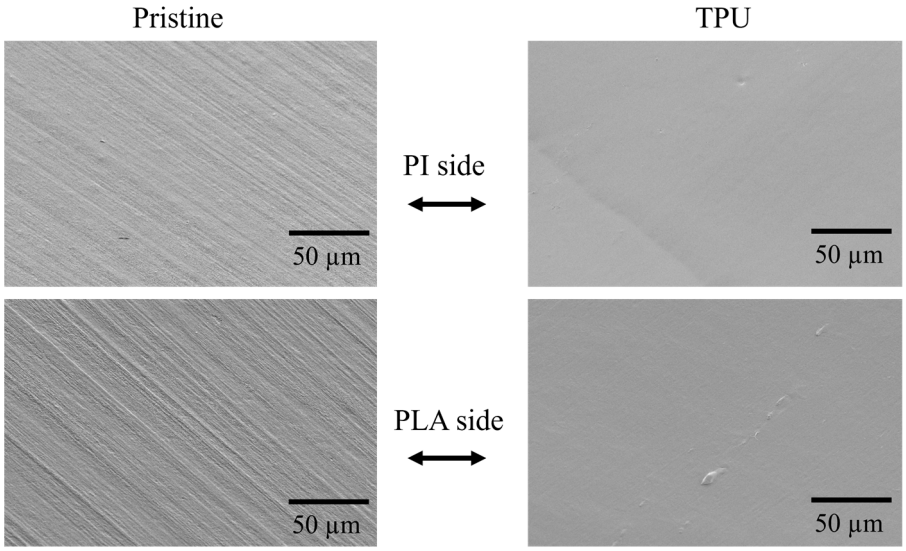

Figure 13. Surface topography change shows the cohesive failure of TPU for Pyralux foil.

5. Conclusions

This study investigated various surface treatments to improve the adhesion between etched copper PI foils and overmolded biopolymers, PLA and PHB, for sustain-

able IME. Drying, PDA coating, PDA + VAC coating, oxygen plasma treatment, and 3-aminopropyltriethoxysilane (APTES) application were compared to a TPU adhesive tie layer lamination technique. The effectiveness of each treatment was evaluated through WCA measurements, SEM analysis of loci failure, XPS analysis of surface chemistry, and 180-degree peel tests to quantify adhesive strength. The results indicate that while surface treatments like PDA coating, PDA + VAC coating, oxygen plasma, and APTES application influence the surface properties of the PI foils, they exhibit varying degrees of improvement in adhesive strength. The most significant improvement in adhesion is achieved through the lamination of a TPU adhesive layer. This approach provides a robust interfacial bond between the PI and the biopolymers, demonstrating its potential for enhancing the durability and reliability of IMEs. The presence of pre-existing CrO_x layers on certain PI foils also influences surface wettability and adhesion, affecting the effectiveness of surface modifications. Chemical treatments alone are insufficient to achieve strong adhesion comparable to TPU lamination. Further research is needed to explore alternative adhesive materials to further enhance the sustainability and performance of biopolymer-based IMEs.

Supplementary Materials: The following supporting information can be downloaded at: https://www.mdpi.com/article/10.3390/coatings15121489/s1, Figure S1. ATR-FTIR spectrum of pristine Upisel foil. Figure S2. ATR-FTIR spectrum of pristine Pyralux foil. Figure S3. ATR-FTIR spectrum of pristine Shenghyi foil. Figure S4. WYKO optical profilometry example images showing surface roughness of pristine Upisel, Pyralux, and Shengyi foils. Figure S5. FEG–SEM images of the Upisel foil (a) after PDA treatment, (b) after PDA + Vacuum treatment. Figure S6. FEG–SEM images of the Pyralux foil (a) after PDA treatment, (b) after PDA + Vacuum treatment. Figure S7. FEG–SEM images of the Shengyi foil (a) after PDA treatment, (b) after PDA + Vacuum treatment. Figure S8. FEG–SEM images of Silicon (a) after PDA treatment, (b) after PDA + Vacuum treatment. Table S1. The functional groups, binding energy, and the area percentage associated with the deconvoluted peaks of the Cs1 detail spectra. The average percentages are calculated from 4 spectra at random spots on the surfaces. Figure S9. High-resolution C1s deconvoluted spectra of PDA and PDA + Vacuum treated silicon reference samples.

Author Contributions: Experiments: Z.F. and D.S.; analysis: Z.F., D.S. and K.L.; writing—original draft preparation: Z.F.; writing—review and editing: D.S., M.C., K.L., R.M., N.D.G., P.B., L.C. and J.V. All authors have read and agreed to the published version of the manuscript.

Funding: This research received no external funding.

Institutional Review Board Statement: Not applicable.

Informed Consent Statement: Not applicable.

Data Availability Statement: The original contributions presented in this study are included in the article/Supplementary Materials. Further inquiries can be directed to the corresponding authors.

Conflicts of Interest: The authors declare no conflicts of interest.

References

1. Beltrão, M.; Duarte, F.M.; Viana, J.C.; Paulo, V. A Review on In-Mold Electronics Technology. *Polym. Eng. Sci.* **2022**, *62*, 967–990. [CrossRef]
2. Bakr, M.; Bossuyt, F.; Vanfleteren, J. The Integration of Electronic Circuits in Plastics Using Injection Technologies: A Literature Review. *Flex. Print. Electron.* **2022**, *7*, 023001. [CrossRef]
3. Rusanen, O.; Simula, T.; Niskala, P.; Lindholm, V.; Heikkinen, M. Injection Molded Structural Electronics Brings Surfaces to Life. In Proceedings of the 2019 22nd European Microelectronics and Packaging Conference & Exhibition (EMPC), Pisa, Italy, 16–19 September 2019; Volume 2019, pp. 1–7. [CrossRef]
4. Abalansa, S.; El Mahrad, B.; Icely, J.; Newton, A. Electronic Waste, an Environmental Problem Exported to Developing Countries: The Good, the Bad and the Ugly. *Sustainability* **2021**, *13*, 5302. [CrossRef]

5. Santato, C.; Alarco, P.J. The Global Challenge of Electronics: Managing the Present and Preparing the Future. *Adv. Mater. Technol.* **2022**, *7*, 3–8. [CrossRef]
6. Fazlali, Z.; Schaubroeck, D.; Cauwe, M.; Ugduler, S.; Van Laere, T.; Manhaeghe, D.; De Meester, S.; Cardon, L.; Vanfleteren, J. Eco-Friendly In-Mold Electronics Using Polylactic Acid. In Proceedings of the 2024 Electronics Goes Green 2024+ (EGG), Berlin, Germany, 18–20 June 2024. [CrossRef]
7. Moshood, T.D.; Nawanir, G.; Mahmud, F.; Mohamad, F.; Ahmad, M.H.; AbdulGhani, A. Sustainability of Biodegradable Plastics: New Problem or Solution to Solve the Global Plastic Pollution? *Curr. Res. Green Sustain. Chem.* **2022**, *5*, 100273. [CrossRef]
8. Available online: https://www.european-bioplastics.org/bioplastics/ (accessed on 22 April 2023).
9. Ramesh Kumar, S.; Shaiju, P.; O'Connor, K.E. Bio-Based and Biodegradable Polymers—State-of-the-Art, Challenges and Emerging Trends. *Curr. Opin. Green Sustain. Chem.* **2020**, *21*, 75–81. [CrossRef]
10. Taib, N.A.A.B.; Rahman, M.R.; Huda, D.; Kuok, K.K.; Hamdan, S.; Bakri, M.K.B.; Julaihi, M.R.M.B.; Khan, A. *A Review on Poly Lactic Acid (PLA) as a Biodegradable Polymer*; Springer: Berlin/Heidelberg, Germany, 2023; Volume 80, ISBN 0123456789.
11. De Luca, S.; Milanese, D.; Gallichi-Nottiani, D.; Cavazza, A.; Sciancalepore, C. Poly (Lactic Acid) and Its Blends for Packaging Application: A Review. *Clean Technol.* **2023**, *5*, 1304–1343. [CrossRef]
12. Singhvi, M.S.; Zinjarde, S.S.; Gokhale, D.V. Polylactic Acid: Synthesis and Biomedical Applications. *J. Appl. Microbiol.* **2019**, *127*, 1612–1626. [CrossRef]
13. Getachew, A.; Woldesenbet, F. Production of Biodegradable Plastic by Polyhydroxybutyrate (PHB) Accumulating Bacteria Using Low Cost Agricultural Waste Material. *BMC Res. Notes* **2016**, *9*, 509. [CrossRef]
14. McAdam, B.; Fournet, M.B.; McDonald, P.; Mojicevic, M. Production of Polyhydroxybutyrate (PHB) and Factors Impacting Its Chemical and Mechanical Characteristics. *Polymers* **2020**, *12*, 2908. [CrossRef] [PubMed]
15. Maddah, H.A. Polypropylene as a Promising Plastic: A Review. *Am. J. Polym. Sci.* **2016**, *6*, 1–11. [CrossRef]
16. Nassajfar, M.N.; Deviatkin, I.; Leminen, V.; Horttanainen, M. Alternative Materials for Printed Circuit Board Production: An Environmental Perspective. *Sustainability* **2021**, *13*, 12126. [CrossRef]
17. Goosey, M. *Polymers in Printed Circuit Board (PCB) and Related Advanced Interconnect Applications*; Springer: Berlin/Heidelberg, Germany, 1999; ISBN 9789048140183.
18. Diaham, S. Polyimide in Electronics: Applications and Processability Overview. *Polyim. Electron. Electr. Eng. Appl.* **2021**, *3*, 2020–2021. [CrossRef]
19. Bakr, M.; Su, Y.; Rezaei, A.; Bossuyt, F.; Vanfleteren, J. Over-Molding of Flexible Polyimide-Based Electronic Circuits. *Flex. Print. Electron.* **2021**, *6*, 025007. [CrossRef]
20. Bakr, M.; Su, Y.; Bossuyt, F.; Vanfleteren, J. Effect of Overmolding Process on the Integrity of Electronic Circuits. In Proceedings of the 2019 22nd European Microelectronics and Packaging Conference & Exhibition (EMPC), Pisa, Italy, 16–19 September 2019. [CrossRef]
21. Lutz, A. *Preparation for Bonding*; Springer: Berlin/Heidelberg, Germany, 2018; Volume 2, ISBN 9783319554112.
22. Raos, G.; Zappone, B. Polymer Adhesion: Seeking New Solutions for an Old Problem#. *Macromolecules* **2021**, *54*, 10617–10644. [CrossRef]
23. Cen-Puc, M.; Schander, A.; Vargasgleason, M.G.; Lang, W. An Assessment of Surface Treatments for Adhesion of Polyimide Thin Films. *Polymers* **2021**, *13*, 1955. [CrossRef]
24. Mashayekhi, F.; Bardon, J.; Westermann, S.; Addiego, F. Adhesion Optimization between Incompatible Polymers through Interfacial Engineering. *Polymers* **2021**, *13*, 4273. [CrossRef]
25. Kafkopoulos, G.; Karakurt, E.; Martinho, R.P.; Duvigneau, J.; Vancso, G.J. Engineering of Adhesion at Metal—Poly (Lactic Acid) Interfaces by Poly (Dopamine): The Effect of the Annealing Temperature. *ACS Appl. Polym. Mater.* **2023**, *5*, 5370–5380. [CrossRef]
26. Fazlali, Z.; Schaubroeck, D.; Cauwe, M.; Cardon, L.; Bauwens, P.; Vanfleteren, J. Polylactic Acid and Polyhydroxybutyrate as Printed Circuit Board Substrates: A Novel Approach. *Processes* **2025**, *13*, 1360. [CrossRef]
27. Lee, H.; Dellatore, S.M.; Miller, W.M.; Messersmith, P.B. Mussel-Inspired Surface Chemistry for Multifunctional Coatings. *Science* **2007**, *318*, 426–430. [CrossRef] [PubMed]
28. Öztoprak, N.; Mehmet, G.; Murat, G. Characterization of Interface, Tensile—Shear, and Vibration Performance of AA2024—T351/PP Composite Stepped—Lap Joint. *Int. J. Adv. Manuf. Technol.* **2025**, *138*, 5537–5553. [CrossRef]
29. Diaham, S.; Locatelli, M.L.; Lebey, T.; Malec, D. Thermal Imidization Optimization of Polyimide Thin Fi Lms Using Fourier Transform Infrared Spectroscopy and Electrical Measurements. *Thin Solid Films* **2011**, *519*, 1851–1856. [CrossRef]
30. Diaham, S.; Locatelli, M.; Khazaka, R. BPDA-PDA Polyimide: Synthesis, Characterizations, Aging and Semiconductor Device Passivation. In *High Performance Polymers-Polyimides Based-From Chemistry to Applications*; IntechOpen: London, UK, 2012.
31. Fang, Y.; Dong, J.; Zhang, D.; Zhao, X.; Zhang, Q. Preparation of High-Performance Polyimide Fibers via a Partial Pre-Imidization Process. *J. Mater. Sci.* **2019**, *54*, 3619–3631. [CrossRef]
32. Ruhland, K.; Haase, N.; Fischer, A. Detailed Examination of Nitrile Stretching Vibrations Relevant for Understanding the Behavior of Thermally Treated Polyacrylonitrile. *J. Appl. Polym. Sci.* **2017**, *134*, 44936. [CrossRef]

33. Qiao, M.; Kong, H.; Ding, X.; Zhang, L.; Yu, M. Effect of Graphene Oxide Coatings on the Structure of Polyacrylonitrile Fi Bers during Pre-Oxidation. *RSC Adv.* **2019**, *9*, 28146–28152. [CrossRef]
34. Wu, C.R.; Liedberg, B. Infrared Reflection-Absorption Spectroscopy of Polyacrylonitrile on Copper and Aluminium Surfaces. *J. Polym. Sci. Part B Polym. Phys.* **1988**, *26*, 1127–1136. [CrossRef]
35. Xiao, G.Z.; Shanahan, M.E.R. Irreversible Effects of Hygrothermal Aging on DGEBA/DDA Epoxy Resin. *J. Appl. Polym. Sci.* **1997**, *69*, 363–369. [CrossRef]
36. Mustata, F.; Tudorachi, N.; Rosu, D. Composites: Part B Curing and Thermal Behavior of Resin Matrix for Composites Based on Epoxidized Soybean Oil/Diglycidyl Ether of Bisphenol A. *Compos. Part B Eng.* **2011**, *42*, 1803–1812. [CrossRef]
37. Liang, W.; Zhao, B.; Zhang, C.; Jian, R.; Liu, D.; Liu, Y. Enhanced Fl Ame Retardancy of DGEBA Epoxy Resin with a Novel Bisphenol-A Bridged Cyclotriphosphazene. *Polym. Degrad. Stab.* **2017**, *144*, 292–303. [CrossRef]
38. Ullah, R.; Li, H.; Zhu, Y. Terahertz and FTIR Spectroscopy of 'Bisphenol A'. *J. Mol. Struct.* **2014**, *1059*, 255–259. [CrossRef]
39. Li, L.; Wu, Q.; Li, S.; Wu, P. Study of the Infrared Spectral Features of an Epoxy Curing Mechanism. *Appl. Spectrosc.* **2008**, *62*, 1129–1136. [CrossRef]
40. Coombs, C.F., Jr. *Printed Circuits Handbook*; McGraw-Hill: New York, NY, USA, 2008; ISBN 0071510796.
41. Zangmeister, R.A.; Morris, T.A.; Tarlov, M.J. Characterization of Polydopamine Thin Films Deposited at Short Times by Autoxidation of Dopamine. *Langmuir* **2013**, *29*, 8619–8628. [CrossRef] [PubMed]
42. Patel, K.; Singh, N.; Yadav, J.; Nayak, J.M.; Sahoo, S.K.; Lata, J.; Chand, D.; Kumar, S.; Kumar, R. Polydopamine films change their physicochemical and antimicrobial properties with a change in reaction conditions. *Phys. Chem. Chem. Phys.* **2018**, *20*, 5744–5755. [CrossRef]
43. Jiang, J.; Zhu, L.; Zhu, L.; Zhu, B.; Xu, Y. Surface Characteristics of a Self-Polymerized Dopamine Coating Deposited on Hydrophobic Polymer Films. *Langmuir* **2011**, *27*, 14180–14187. [CrossRef]
44. Bogdan, D.; Grosu, I.; Filip, C. Applied Surface Science How Thick, Uniform and Smooth Are the Polydopamine Coating Layers Obtained under Different Oxidation Conditions? An in-Depth AFM Study. *Appl. Surf. Sci.* **2022**, *597*, 153680. [CrossRef]
45. Garbassi, F.; Morra, M.; Occhiello, E. Polymer Surfaces from Physics to Technology. *IEEE Electr. Insul. Mag.* **1999**, *15*, 36–37. [CrossRef]
46. Amin, M.H.; Patel, K.D.; Patel, N.A.; Patel, D.Y.; Chauhan, K.V. Study the Influence of Deposition Parameter on Structure & Wettability Properties of Chromium Oxide Coating Deposited by Reactive RF Magnetron Sputtering on GFRP Composite. *Mater. Today Proc.* **2021**, *50*, 2381–2386. [CrossRef]
47. Sundriyal, P.; Pandey, M.; Bhattacharya, S. Plasma-Assisted Surface Alteration of Industrial Polymers for Improved Adhesive Bonding. *Int. J. Adhes. Adhes.* **2020**, *101*, 102626. [CrossRef]
48. Schaubroeck, D.; Vercammen, Y.; Van Vaeck, L.; Vanderleyden, E.; Dubruel, P.; Vanfleteren, J. Surface Characterization and Stability of an Epoxy Resin Surface Modified with Polyamines Grafted on Polydopamine. *Appl. Surf. Sci.* **2014**, *303*, 465–472. [CrossRef]
49. Ghobeira, R.; Philips, C.; Declercq, H.; Cools, P.; De Geyter, N.; Cornelissen, R.; Morent, R. Effects of Different Sterilization Methods on the Physico-Chemical and Bioresponsive Properties of Plasma-Treated Polycaprolactone Films. *Biomed. Mater.* **2017**, *12*, 015017. [CrossRef]
50. Feinberg, H.; Hanks, T.W. Polydopamine: A Bioinspired Adhesive and Surface Modification Platform. *Polym. Int.* **2022**, *71*, 578–582. [CrossRef]
51. Sun, X.; Bu, J.; Liu, W.; Niu, H.; Qi, S.; Tian, G.; Wu, D. Surface Modification of Polyimide Fibers by Oxygen Plasma Treatment and Interfacial Adhesion Behavior of a Polyimide Fiber/Epoxy Composite. *Sci. Eng. Compos. Mater.* **2017**, *24*, 477–484. [CrossRef]
52. Yan, C.; Tong, H.; Liu, C.; Ye, X.; Yuan, X.; Xu, J.; Li, H. Activation of Polyimide by Oxygen Plasma for Atomic Layer Deposition of Highly Compact Titanium Oxide Coating. *Nanotechnology* **2024**, *35*, 265704. [CrossRef] [PubMed]